DUDLEY KNOX LIBRARY
SCHOOL
3002

NAVAL POSTGRADUATE SCHOOL
Monterey, California

THESIS

R2198

THE MICROSTRUCTURAL BASIS OF DAMPING
IN HIGH DAMPING ALLOYS

by

Peter Frederick Rappeline

September 1989

Thesis Advisor: Jeff Perkins

Approved for public release; distribution is unlimited

REPORT DOCUMENTATION PAGE

Form Approved
OMB No 0704-0188

1a REPORT SECURITY CLASSIFICATION UNCLASSIFIED	1b RESTRICTIVE MARKINGS
2a SECURITY CLASSIFICATION AUTHORITY	3 DISTRIBUTION / AVAILABILITY OF REPORT Approved for public release; distribution is unlimited
2b DECLASSIFICATION / DOWNGRADING SCHEDULE	
4 PERFORMING ORGANIZATION REPORT NUMBER(S)	5 MONITORING ORGANIZATION REPORT NUMBER(S)
6a NAME OF PERFORMING ORGANIZATION Naval Postgraduate School 6b OFFICE SYMBOL (If applicable) Code 69	7a NAME OF MONITORING ORGANIZATION Naval Postgraduate School
6c. ADDRESS (City, State, and ZIP Code) Monterey, California 93943-5000	7b ADDRESS (City, State, and ZIP Code) Monterey, California 93943-5000
8a NAME OF FUNDING / SPONSORING ORGANIZATION 8b OFFICE SYMBOL (If applicable)	9 PROCUREMENT INSTRUMENT IDENTIFICATION NUMBER
8c. ADDRESS (City, State, and ZIP Code)	10 SOURCE OF FUNDING NUMBERS PROGRAM ELEMENT NO / PROJECT NO / TASK NO / WORK UNIT ACCESSION NO

11 TITLE (Include Security Classification)

THE MICROSTRUCTURAL BASIS OF DAMPING IN HIGH DAMPING ALLOYS

12 PERSONAL AUTHOR(S)
Rappeline, Peter F.

13a TYPE OF REPORT	13b TIME COVERED	14 DATE OF REPORT (Year, Month, Day)	15 PAGE COUNT
Master's Thesis	FROM _____ TO _____	1989, September	54

16 SUPPLEMENTARY NOTATION
The views expressed in this thesis are those of the author and do not reflect the official policy or position of the Department of Defense or the U.S. Government.

17 COSATI CODES			18 SUBJECT TERMS (Continue on reverse if necessary and identify by block number)
FIELD	GROUP	SUB-GROUP	Damping Alloys; CuAlNi, CuMn; INCRAMUTE; Strain-Dependent Damping

19 ABSTRACT (Continue on reverse if necessary and identify by block number)

The microstructural mechanisms responsible for material damping are analyzed, with emphasis on those mechanisms responsible for the behavior in high damping alloys. A Cu-Al-Ni alloy is metallurgically characterized using transmission electron microscopy and differential scanning calorimetry. The microstructural characterization of the Cu-Mn alloy INCRAMUTE is refined using high resolution transmission electron microscopy and high resolution energy-dispersive x-ray spectroscopy. A qualitative theory for the strain dependence of damping capacity is given.

20 DISTRIBUTION / AVAILABILITY OF ABSTRACT ☒ UNCLASSIFIED/UNLIMITED ☐ SAME AS RPT ☐ DTIC USERS	21 ABSTRACT SECURITY CLASSIFICATION Unclassified
22a NAME OF RESPONSIBLE INDIVIDUAL Prof. Jeff Perkins	22b TELEPHONE (Include Area Code) (408) 646-2216 22c OFFICE SYMBOL Code 69Ps

T245545

Approved for public release; distribution is unlimited

The Microstructural Basis of Damping in High Damping Alloys

by

Peter Frederick Rappeline
Lieutenant Commander, United States Navy
B.S., University of Rhode Island, 1972

Submitted in partial fulfillment of the
requirements for the degree of

MASTER OF SCIENCE IN MECHANICAL ENGINEERING

from the

NAVAL POSTGRADUATE SCHOOL
September 1989

ABSTRACT

The microstructural mechanisms responsible for material damping are analyzed, with emphasis on those mechanisms responsible for the behavior in high damping alloys. A Cu-Al-Ni alloy is metallurgically characterized using transmission electron microscopy and differential scanning calorimetry. The microstructural characterization of the Cu-Mn alloy INCRAMUTE is refined using high resolution transmission electron microscopy and high resolution energy-dispersive x-ray spectroscopy. A qualitative theory for the strain dependence of damping capacity is given.

LD
P2198
C.1

TABLE OF CONTENTS

I. INTRODUCTION ---------- 1

II. BACKGROUND ---------- 2

A. THE NATURE OF ELASTIC RESPONSE IN HIGH DAMPING ALLOYS ---------- 2

B. MICROSTRUCTURAL DAMPING MECHANISMS ---------- 3

C. THE STRESS-STRAIN HYSTERESIS LOOP ---------- 9

D. SPECIFIC DAMPING CAPACITY ---------- 11

III. OBJECTIVES ---------- 12

IV. EXPERIMENTAL PROCEDURE ---------- 13

A. Cu-Al-Ni-Mn-Ti ---------- 13

B. CuMn (INCRAMUTE) ---------- 15

V. RESULTS AND DISCUSSION ---------- 16

A. TRANSMISSION ELECTRON MICROSCOPE (TEM) EXAMINATION OF Cu-Al-Ni-Mn-Ti ---------- 16

B. DIFFERENTIAL SCANNING CALORIMETRY (DSC) OF Cu-Al-Ni-Mn-Ti ---------- 20

C. HIGH RESOLUTION ELECTRON MICROSCOPE (HREM) EXAMINATION OF INCRAMUTE ---------- 22

D. STRAIN DEPENDENCE IN DAMPING ---------- 25

VI. CONCLUSIONS AND RECOMMENDATIONS ---------- 28

A. CONCLUSIONS ---------- 28

B. RECOMMENDATIONS ---------- 28

APPENDIX A: CHEMICAL COMPOSITION OF Cu-Al-Ni-Mn-Ti ---- 30

APPENDIX B: Cu-Al-3Ni PHASE DIAGRAM ---------- 31

APPENDIX C: SPECIFIC DAMPING CAPACITY VS. CYCLIC STRAIN AMPLITUDE FOR VARIOUS ALLOYS ------- 32

APPENDIX D: COMPARISON OF DSC AUSTENITIC PEAKS FOR 150°C AND 200°C AGED Cu-Al-Ni-Mn-Ti ------ 42

LIST OF REFERENCES ---------- 43

INITIAL DISTRIBUTION LIST ---------- 44

LIST OF FIGURES

2.1 Stress-Strain Hysteresis Loop ---------- 10

5.1 Spear-Shaped Morphology in Cu-Al-Ni-Mn-Ti -------- 17

5.2 Individual Variant Linear Substructural Detail in Cu-Al-Ni-Mn-Ti ---------- 18

5.3 Antiphase Domain Boundaries (APB's)in Cu-Al-Ni-Mn-Ti ---------- 19

5.4 X_L Phase Precipitate ---------- 21

5.5 High Resolution Transmission Electron Micrograph of INCRAMUTE ---------- 24

A.1 Anamet Laboratories Assay of Cu-Al-Ni-Mn-Ti ------ 30

B.1 Cu-Al-3Ni Phase Diagram ---------- 31

C.1 SDC vs. Strain--FeCrMo ---------- 32

C.2 SDC vs. Strain--TiNi ---------- 33

C.3 SDC vs. Strain--INCRAMUTE ---------- 34

C.4 SDC vs. Strain--CuZnAl ---------- 35

C.5 SDC vs. Strain--Cu-Al-Ni-Mn-Ti 800C30MIN/WQRT ---- 36

C.6 SDC vs. Strain--Cu-Al-Ni-Mn-Ti 800C30MIN/WQRT/ 150C1HR/WQRT ---------- 37

C.7 SDC vs. Strain--Cu-Al-Ni-Mn-Ti 800C30MIN/WQRT/ 200C1HR/WQRT ---------- 38

C.8 SDC vs. Strain--Cu-Al-Ni-Mn-Ti 800C30MIN/WQ100C/ WQRT ---------- 39

C.9 SDC vs. Strain--Cu-Al-Ni-Mn-Ti 800C30MIN/WQ100C/ WQRT/150C1HR/WQ100C/WQRT ---------- 40

C.10 SDC vs. Strain-Cu-Al-Ni-Mn-Ti 800C30MIN/WQ100C/WQRT/200C1HR/WQ100C/WQRT ---------- 41

D.1 Austenitic Endothermic Peaks in Aged Cu-Al-Ni-Mn-Ti ---------- 42

ACKNOWLEDGMENTS

The author wishes to express his deep appreciation to Prof. Jeff Perkins, Prof. Tadayoshi Yamashita, Prof. Youji Taneda, Mr. Robert Hafley and Mr. Thomas Kellogg for their assistance in the completion of this work.

I. INTRODUCTION

The absorption of vibrational energy is a fundamental characteristic of all materials. However, the degree of absorption is quite variable. Most metals absorb only a very small proportion of the vibrational energy to which they are exposed. As a result, metallic machine components tend to inherently transfer a large proportion of vibrational energy from one to another, and to the machinery casing and support structures. This contributes to wear, fatigue and noise.

Certain metallic alloys, however, do absorb a large proportion of the incident vibrational energy. These high damping alloys (sometimes called HIDAMETS or "quiet metals") possess unique microstructural mechanisms of energy absorption. The elastic response of these mechanisms can absorb several orders of magnitude more energy than those of conventional (non-damping) metals. Thus machinery components made from these metals have the possibility of damping rather than transferring machinery vibrations and thus reducing the detrimental effects of wear, fatigue and noise.

II. BACKGROUND

A. THE NATURE OF ELASTIC RESPONSE IN HIGH DAMPING ALLOYS

Elastic response in a material is characterized by a spontaneous return to the original shape following the removal of a mechanical load. In order for this to occur, the microstructure of the material must be capable of some sort of physical movement or rearrangement.

If the response of the material is to be completely elastic, there can be no plastic deformation, and any microstructural adjustment which occur upon loading must be completely atomistically reversed upon unloading. This implies that completely elastic microstructural movements can only be achieved at a stress lower than the critical stress for dislocation movement (or other plastic deformation mechanisms, such as twinning), i.e., below a "yield stress." The elastic recovery also requires the presence of a restoring force that drives the microstructure to its original configuration upon unloading.

The microstructural mechanisms which meet the criteria for elastic reversibility are of four general types:

1. Elastic bond stretching within the material lattice.
2. Elastic movement of dislocations.
3. Stress-induced phase transformation.
4. Stress-induced boundary migration.

The mechanical efficiency of these various mechanisms is greatly different. It may be noted that the latter two exhibit a significantly greater degree of elastic hysteresis which is a key to high material damping. The high damping microstructural features respond reversibly with respect to restoration of original shape, but are highly irreversible with respect to mechanical energy balance. Therefore, we may note that a microstructure which is an efficient damper of energy is conversely an inefficient machine for the transfer of vibrational energy.

The descriptive term "internal friction" is commonly used in reference to material damping. According to the common meaning of this term, energy is dispersed within the material, usually in the form of heat, due to irreversibilities ("frictions") in the motions of its microstructural features.

B. MICROSTRUCTURAL DAMPING MECHANISMS

1. Lattice Damping

The crystallographic lattice accommodates strain by increasing the average spacing between lattice points in the direction of the strain. Thus the total strain is accommodated by a large number of atomistic-scale increments. This mechanism provides a very small amount of damping. In fact the lattice of a perfect crystal can be modeled as a set of point masses connected by perfect springs with a high degree

of accuracy [Ref. 1]. Lattice damping is negligible with respect to other mechanisms.

2. Dislocation Damping

Dislocations are line defects in the crystal structure of a metal. The movement of a dislocation from one equilibrium position to another causes slip in the crystal structure and plastic deformation in the metal. Energetically, the dislocation may be considered as residing within a potential well. If the stress is below the yield stress the dislocation will return to its original equilibrium position upon removal of the stress. Stresses above the yield stress move the dislocation out of the potential well and into a new equilibrium position. The movement to this new equilibrium position, termed slip, produces plastic deformation [Ref. 2].

The movement of the dislocation within (but not out of) the potential well dissipates energy, i.e., causes damping, and is elastic in that the original shape is restored upon unloading.

The amount of damping associated with this mechanism is much greater than that of lattice damping, but much less than that of stress-induced phase transformation or stress-induced boundary migration.

3. Stress-Induced Phase Transformation

It is possible in certain alloys (e.g., Cu-Al-Ni and Cu-Zn-Al) to induce a phase transformation by the application

of stress [Ref. 3]. The transformation is from an "austenitic" parent phase to a "martensitic" product phase. This transformation is diffusionless and is characterized by the cooperative movement of atoms in a given section of crystal. Removal of the stress may allow atomistic reversion to the parent phase and hence a unique form of "elasticity." Martensitic phases so formed are termed pseudoelastic martensites. The cooperative movement of atoms causes large internal friction and high damping. The temperature range in which this transformation can be induced is typically fairly narrow and, therefore, may not correspond with normal machine operating temperatures. Thus, although it produces considerable damping, this effect may not be practical for applications in general.

4. Stress-Induced Boundary Migration

The movement of boundaries during elastic deformation is the primary mechanism of energy dissipation in damping alloys. The boundaries are of two general types: (1) Boundaries between and within martensitic plates; and (2) Ferromagnetic or antiferromagnetic domain boundaries.

a. Martensitic Plate Boundaries

Thermoelastic martensite is produced by quenching from above a material dependent high temperature (austenite finish temperature A_f) to below a material dependent low temperature (martensite finish temperature M_f). This

thermoelastic martensite is related to the pseudoelastic martensite previously discussed [Ref. 4].

The morphology of the phase so produced is generally in the form of oblong or ellipsoid shapes, usually termed "plates." The orientation of these ellipsoids in the as-quenched condition is quite variable (although a specific type of crystallographic habit plane will be used).

Under stress, certain plates which are favorably aligned with the direction of stress will grow, while other plates will correspondingly shrink. The movement of these plate boundaries represents a local atomistic reconfiguration of the material, from the configuration outside of to that within the growing plate. Thus the boundaries may be thought of as reorientation boundaries. Through a given range of stress this process is atomistically reversed upon unloading, hence it is a unique form of elasticity. Such reorientations produce considerable internal friction and hence they represent a powerful damping mechanism.

Strain above a material dependent elastic strain limit is retained upon unloading. This strain is recoverable (up to a second material dependent strain limit) by heating. When heated to above A_f, the material transforms back to the parent austenitic phase and the original shape is restored. The recovery of shape from this apparent (false) plasticity is termed the shape memory effect. Alloys which exhibit this

behavior are termed martensitic shape memory alloys (MARMEM) [Ref. 5].

b. Ferromagnetic/Antiferromagnetic Domain Boundaries

Alloys containing transition elements with strong unbalanced magnetic moments (e.g., Fe and Mn) may exhibit an internal magnetic structure. This structure, termed the magnetic lattice, is made up of substructural entities called domains. The magnetic moment vectors within each domain may be parallel (ferromagnetic) or antiparallel (antiferromagnetic) and the boundaries between domains are called domain or Bloch walls. The magnetization within each domain is at saturation. The direction of the parallel or antiparallel magnetic moment vectors is random from domain to domain and the net magnetization of the material is zero. The free energy of the domained structure is therefore less than the undomained structure. This free energy difference is the driving force for domain formation [Ref. 6:p. 37-6].

The particular orientation within each domain is the result of preferred or "easy" directions of magnetization within the sub-lattice elements of the crystal. The energy associated with the difference between orientations is termed anisotropy energy.

A second interaction termed the exchange field tends to line up the magnetic moments parallel to each other. This produces the parallel or antiparallel orientation within each domain. The operation of this field is strongly

temperature dependent. Thermal agitation interferes with the parallel or antiparallel ordering of the exchange field. Thus, the ordering disappears above a material specific characteristic temperature. This temperature is called the Curie temperature for ferromagnetic ordering, and the Neel temperature for antiferromagnetic ordering.

A third interaction, termed magnetostriction, is magneto-mechanical in nature. The alignment of magnetic moments within a domain increases the crystal lattice spacing in the direction of magnetization, creating a localized expansion of the lattice. This causes compressive stresses at the domain interfaces. The distribution of the domain walls is a function of these three interactions [Ref. 6:pp.37-6--37-9].

The internal magnetic structure and width of the domain wall are determined from the solution to the Heisenberg equation [Ref. 7:p. 493]. The free energy of the wall is lowest when it consists of small increments of change across many lattice planes, that is, if the wall is "thicker." The thickness of the wall is a function of the anisotropy energy difference of the neighboring domains. A larger anisotropy difference will produce a thicker wall. That is a larger number of steps will be needed to gradually accommodate a greater change. In iron the domain walls are approximately 300 lattice planes (1000 Å) thick [Ref. 7:p. 492].

At temperatures below the Curie or Neel temperatures the ferromagnetic/antiferromagnetic domains form. Their configuration, size and wall thickness are determined by the equilibration of exchange energy, anisotropy energy and magnetostriction.

Under stress the domains with magnetic moments aligned in the direction of the stress grow at the expense of those not so aligned. This occurs because the magnetostrictive component of the reorientation is reduced by the strain in the lattice. The anisotropy and exchange energies are unchanged. The domain wall moves perpendicular to the stress axis to a new equilibrium position. Removal of the external stress returns the domains to their original configuration, hence it is elastic. The movement of the domain walls absorbs energy and causes damping.

C. THE STRESS-STRAIN HYSTERESIS LOOP

Material damping can be illustrated by comparing the loading curve to the unloading curve in a stress vs. strain tension test. The loading and unloading trajectories have the same shape but the unloading trajectory is shifted to the right, thus forming a loop (Figure 2.1). This loop structure around the nominal straight line elastic trajectory is indicative of the time-dependent microstructural mechanisms associated with damping [Ref. 8:p. 6]. The area contained within the loop is directly proportional to the amount of

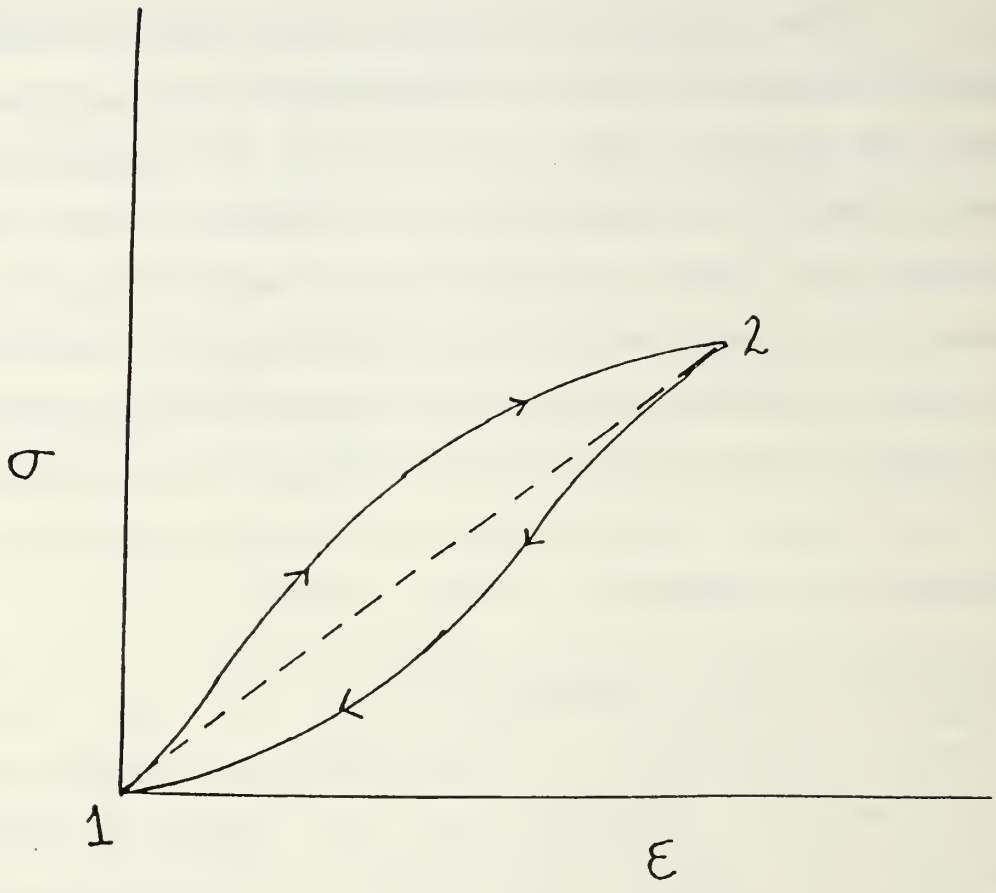

--- Nominal Elastic Trajectory
1→2 Loading Trajectory
2→1 Unloading Trajectory

Figure 2.1 Stress-Strain Hysteresis Loop

damping. All metals exhibit some degree of stress-strain hysteresis but in normal metals the area is negligibly small.

Physically the loop can be modeled with a spring and dashpot system. The loop increases in area as the damping coefficient of the dashpot is increased [Ref. 8:p. 7].

This phenomenon is a direct analogue of magnetic hysteresis, with stress corresponding to magnetizing force, strain to magnetization and elastic modulus to permeability [Ref. 6:p. 36-6].

D. SPECIFIC DAMPING CAPACITY

Specific damping capacity (SDC) is a measure of energy dissipation during the cyclic elastic response of a material. It may be defined for measurements made in free decay or forced vibration. Energetically it is the ratio of the energy decay per cycle to the peak potential energy. Roey [Ref. 9:p. 2] and Reskusich [Ref. 10:pp. 14-19] give a detailed development of SDC.

Normal metallic alloys have SDC's in the range of 0.2-10%, while high-damping alloys have SDC's on the order of 40% [Ref. 11].

III. OBJECTIVES

Research on high damping alloys has been conducted at the Naval Postgraduate School for several years. This continuing program of research has two broad objectives:

1. To measure the specific damping capacity of high damping alloys under varying conditions of strain and temperature.

2. To characterize the microstructure of high damping alloys and by these characterizations to explain the differences observed in SDC.

The specific goals of this thesis are:

1. To metallurgically characterize the microstructure of a Cu-Al-Ni-Mn-Ti alloy.

2. To determine the transformation temperatures of the γ' martensitic phase of this alloy (A_s, M_s, M_f).

3. To refine the microstructural characterization of the Cu-Mn alloy INCRAMUTE.

4. To suggest an overall theory for strain dependence in damping alloys.

IV. EXPERIMENTAL PROCEDURE

A. Cu-Al-Ni-Mn-Ti

The copper, aluminum, nickel, manganese, titanium alloy under test was provided to the Naval Postgraduate School by Memory Metals Inc., of Norwalk, CT. The material was assayed by Anamet Laboratories of Hayward, CA, to verify the chemical composition provided by Memory Metals Inc.

The verified composition (wt%) is:

Cu	Al	Ni	Mn	Ti	Remainder
80.1	11.87	4.95	1.03	1.05	0.2

The Anamet Laboratories report comprises Appendix A.

The approximate phase diagram recommended for use by Memory Metals, Inc., comprises Appendix B. No exact phase diagram for this alloy exists. The heat treatment recommendation from Memory Metals of heating to 800°C, holding for 30 min. and water-quenching to room temperature was based on this phase diagram. The beta (ß) phase is the parent phase for the gamma-prime (γ') thermoelastic martensitic product phase. For the 12% Al composition, 800°C is within the ß phase. The M_S equation on the phase diagram gives an M_S temperature for this composition of 187°C. Memory Metals believed this equation to be applicable. They also believed the M_f to be above room temperature. Therefore quenching to room temperature was

recommended to produce a complete trans-formation to the γ' martensitic damping phase.

All specimens were heated to 800°C and held for 30 min. The specimens were then quenched in water. Some of these were quenched directly to room temperature. Others were quenched to 100°C (boiling water) held for 15 sec., then quenched to room temperature. The 100°C intermediate step was introduced to eliminate warping which was observed for a direct room temperature quench. Memory Metals recommended a post quench aging treatment of 150°C for 1 hr. (followed by a quench to room temperature). This heat treatment was designed to raise the transformation temperature (A_S) and thereby increase the temperature at which the martensitic phase can be used. This recommended aging treatment was performed. In addition, an aging treatment at 200°C for 1 hr. (followed by a quench to room temperature) was performed to assess the effect of increased aging temperature. The specimens that had been intermediately quenched to 100°C from 800°C were also intermediately quenched to 100°C after the 150°C or 200° aging. This produced a total of six conditions:

1. 800C30MIN/WQRT.
2. 800C30MIN/WQRT/150C1HR/WQRT.
3. 800C30MIN/WQRT/200C1HR/WQRT.
4. 800C30MIN/WQ100C/WQRT.

5. 800C30MIN/WQ100C/WQRT/150C1HR/WQ100C/WQRT.

6. 800C30MIN/WQ100C/WQRT/200C1HR/WQ100C/WQRT.

Transmission electron microscope (TEM) specimens were prepared for each of the six conditions. This was accomplished by cutting thin (0.012 in.) foils out of which were punched 3mm (0.118 in.) discs. The discs were hand-sanded then cleaned in an acetone bath in an ultrasonic cleaner. The specimens were then electropolished with a 50% phosphoric acid 50% water solution at room temperature, 10-12 V.

The same technique was followed for differential scanning calorimetry (DSC) specimen preparation with the exception that the specimens were not electropolished. For the DSC analysis a scanning rate of 2.5°C per minute and a chart speed of 10 millimeters per minute were used. Pure Al was used as the comparison metal.

B. Cu-Mn (INCRAMUTE)

The Cu-Mn (INCRAMUTE) transmission electron micrograph used in this thesis was provided by Professor Youji Taneda, visiting scholar from the National Defense Academy, Japan. The specimens from which they were produced were solution treated at 800°C for 2 hr. and quenched to room temperature.

Prof. Taneda also provided high resolution energy dispersion x-ray spectroscopic analysis of the specimens.

V. RESULTS AND DISCUSSION

A. TRANSMISSION ELECTRON MICROSCOPE (TEM) EXAMINATION OF Cu-Al-Ni-Mn-Ti

Representative transmission electron micrographs, typical of all six heat treatments, are shown in Figures 5.1 through 5.3. Figure 5.1 is an example of the overall structure, while Figures 5.2 and 5.3 show substructural details at greater magnification. The spear-shaped morphology seen in Figure 5.1, which is characteristic of the γ' (2H) martensite, was observed in all specimens. The individual variants all exhibit a linear substructural pattern indicative of stacking faults as seen in Figure 5.2. In addition, they all exhibit numerous twinning and microtwin orientations. All specimens contained small amounts of retained austenitic parent (ß) phase.

The crystal structure of the γ' martensitic product phase is ordered orthohombic with lattice parameters: a = 4.382Å, b = 5.356Å, c = 4.222Å. The crystal structure of the ß parent phase is the ordered DO_3 structure with lattice parameter 5.84Å. The ordered structure of the product phase is dictated by the ordered structure of the parent phase. The retention of antiphase domains in the austenitic structure is shown in Figure 5.3. Antiphase domain boundaries (APB's) were observed

Figure 5.1 Spear-shaped Morphology in Cu-Al-Ni-Mn-Ti. Numerous Twin and Microtwin Orientations Are Visible (24.6 KX)

Figure 5.2 Individual Variant Substructural Detail in Cu-Al-Ni-Mn-Ti. Linear Horizontal Pattern Is Indicative of Stacking Faults (145 KX)

Figure 5.3 Antiphase Domain Boundaries (APB's) in Cu-Al-Ni-Mn-Ti (178 KX)

in all specimens. The size and distribution of the APB's was the same in all specimens.

All specimens contained a very widely dispersed precipitate (see Figure 4.4a). The precipitate exhibited a spherical morphology (Figure 4.4b). This precipitate is known as the X_L phase. The crystal structure is $L2_1$ with lattice parameter 5.978Å.

There was no discernible difference in the micrographs of the six heat treatment conditions. They all exhibit γ' martensitic phase with a small amount of ß phase and a small amount of precipitate (X_L) phase. It is felt that the small amounts of the ß and X_L phases should have little or no effect on the mechanical properties of the microstructure.

B. DIFFERENTIAL SCANNING CALORIMETRY (DSC) OF Cu-Al-Ni-Mn-Ti

The A_S temperature for the unaged condition was 187°C. The A_S temperature for both the 150°C and 200°C aged conditions was 202°C. The M_S temperature for the unaged condition was 129°C. The M_S temperature for both aged conditions was 143°C. The M_f temperature for the unaged condition was 117°C. The M_f temperature for both aged conditions was 129°C. Thus the aging treatment which was recommended (150°C, 1hr.) produced the expected increased in A_S temperature. The 200°C aging produced the same sort of shift of transformation temperatures.

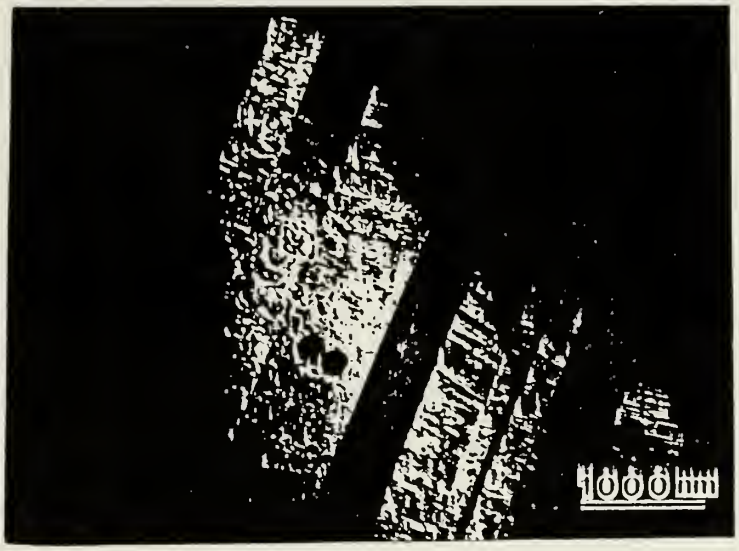

(a) Representative Size and Dispersion of X_L Phase Precipitate in Cu-Al-Ni-Mn-Ti

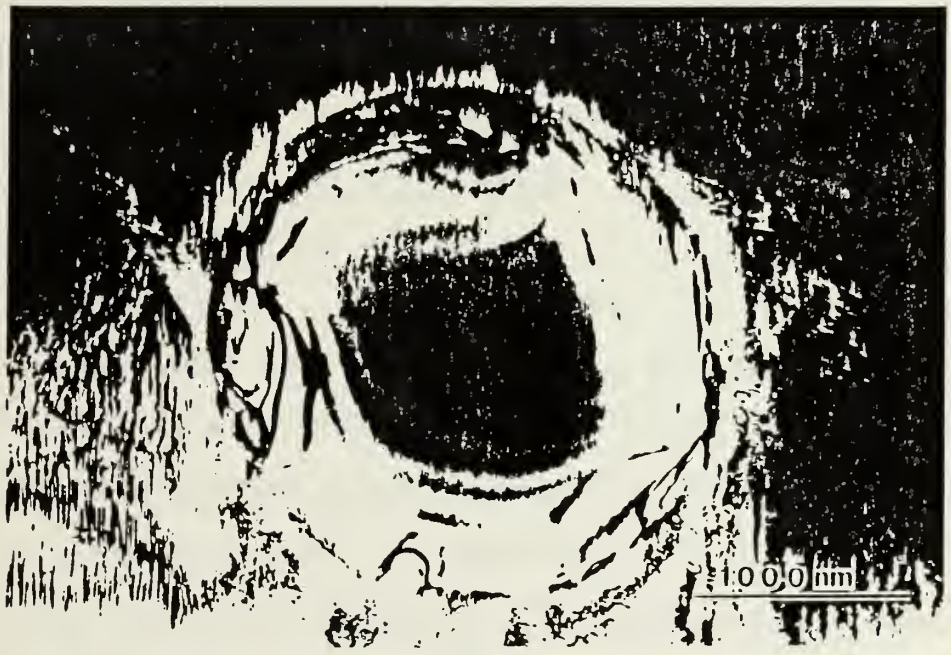

(b) Large X_L Phase Precipitate Particle in Cu-Al-Ni-Mn-Ti

Figure 5.4 X_L Phase Precipitate

However the specific transformation signatures of the two aging treatments during the austenitic transformation were quite different. The individual endothermic peaks were sharper and higher in the 200°C aged specimen, while those in the 150°C aged specimen were broader and flatter (see Appendix D). The total area under the peaks was approximately the same in the two aged cases. The unaged austenitic peaks were of a much smoother character.

This difference in signature may be associated with some subtle difference in the internal friction. For example, the more distinct bursts evident in the 200°C treatment may be related to atomic movements which contribute to higher damping. Roey [Ref. 9:pp. 10-11] observed marginally better SDC in the 200°C aged specimen. This would also indicate a slightly elevated internal friction. As stated above, no structural differences were observed at the scale of observation possible in the conventional TEM micrographs presented here.

C. HIGH RESOLUTION ELECTRON MICROSCOPE ANALYSIS OF INCRAMUTE

Mayes [Ref. 12] performed a transmission electron microscopic analysis of INCRAMUTE. Over a range of aging conditions an aligned {110} "tweed" contrast pattern was observed. Also, a unique dynamic behavior termed "flickering" was noticed as associated with a V-shaped geometric feature in the tweed pattern. Mayes suggested that these V-shaped

features might be embedded in Mn-rich regions, and hence be FCT in structure, with the flickering being a manifestation of the FCT c-axis changing from one orientation to another. Thus, the flickering could be associated with an energy-absorbing microstructural movement. The extremely fine scale (10 nm) and the resolution limit of the TEM in use precluded observing the level of detail necessary to test this hypothesis. In addition Mayes had no instrument available to map the Mn concentration variation on so fine a scale.

In connection with the present work, Prof. Taneda used high resolution TEM to examine specimens after overaging heat treatment (to produce a slightly larger and more coarse V-shaped structure). An Akashi high resolution electron microscope (HREM) was used. In addition, this microscope was equipped with a high resolution energy dispersion x-ray spectrometer (HREDX), which enabled the Mn concentration variation to be mapped to within 3 nm.

The HREDX analysis determined that the regions which contain the V-shaped features are indeed Mn-rich.

An example of the HREM results is shown in Figure 5.5. The dark dashed region bracketed by the arrows is Mn-rich. The fringe pattern marked by the arrows is FCT. The difference in directions of this pattern (marked by the arrows) is indicative of different FCT c-axis orientations. This forms a very small pair of twin-related regions. The matrix structure surrounding these regions is FCC.

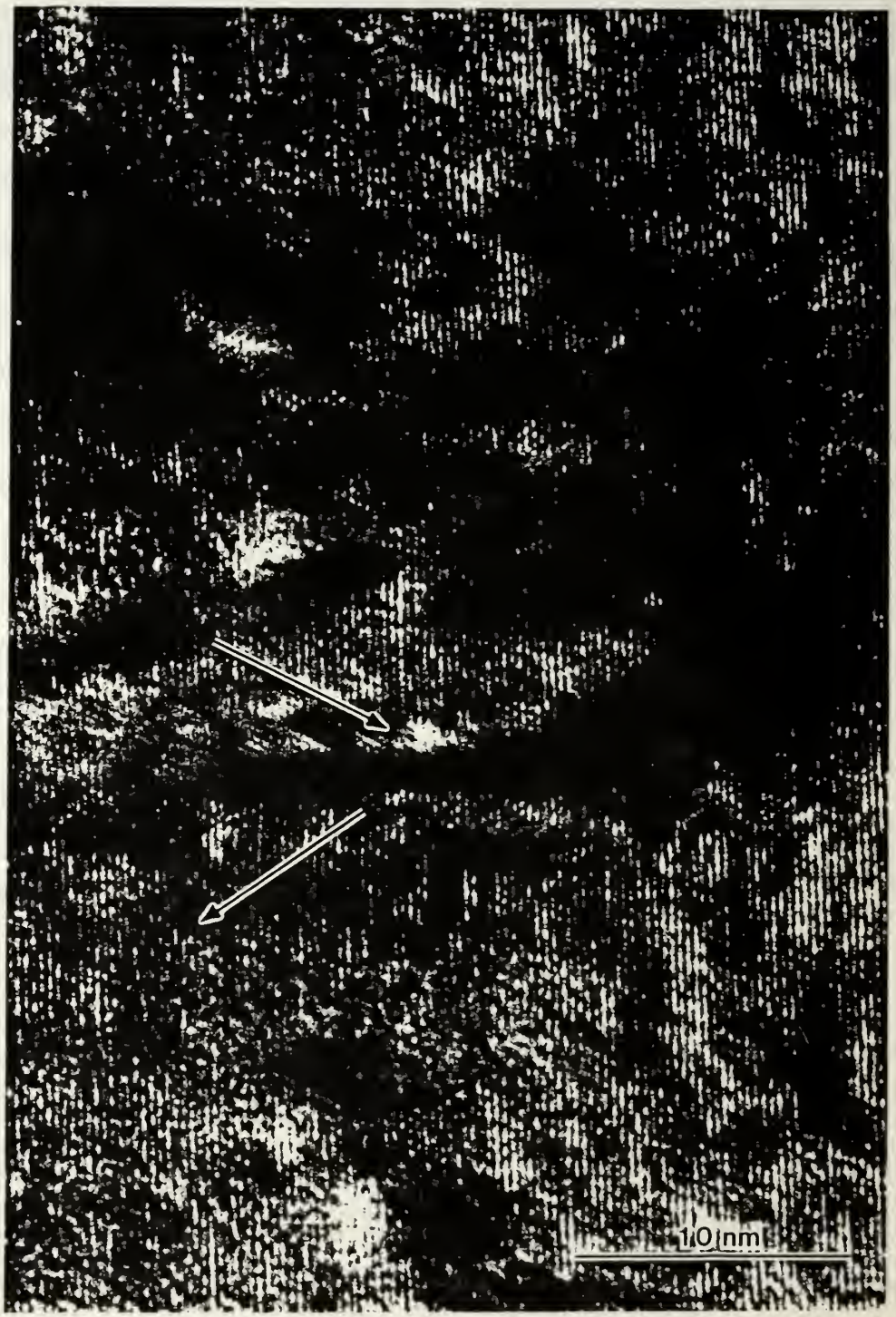

Figure 5.5 High Resolution Transmission Electron Micrograph of INCRAMUTE. Twin-like Feature Marked by Arrows (4000 KX)

Thus the V-shaped regions have been determined to be structured in the manner suggested by Mayes. The locally elevated Mn concentration produces the FCT crystal structure upon cooling; this structure forms with different c-axis orientations, creating twin-like boundaries between self-accommodating regions. The movement of the boundary under stress, characterized by the shift in c-axis orientation, produces flickering and damping.

In addition, the Mn atoms in Cu-Mn exhibit antiferromagnetic coupling below the Neel temperature. This fact and the anisotropy across the twin boundary suggest that this interface, which comprises an antiferromagnetic domain wall, is an excellent candidate for high damping.

Thus this structure simultaneously provides two interrelated mechanisms of damping, namely (1) the atomic adjustments of twin boundary movement, and (2) antiferromagnetic adjustments during domain boundary movement. (It should be noted that the boundary between differently oriented FCT regions is simultaneously a twin boundary and an antiferromagnetic domain boundary in this case.)

D. STRAIN DEPENDENCE IN DAMPING

The strain dependence of specific damping capacity has been studied by Roey [Ref. 9:pp. 8-12]. Graphs of cyclic strain amplitude vs. SDC given by Roey comprise Appendix C.

It is noted that the curves are of two forms. All of the martensitic alloys (TiNi, CuAlNi, CuZnAl) and the quasi-martensitic INCRAMUTE are strain dependent at low strain amplitudes and strongly strain dependent above a (material-specific and well-defined) strain threshold. The Fe-Cr-Mo is strain dependent throughout the entire measured ranged; the SDC of this alloy increases with increasing strain amplitude reaching a peak at approximately one microstrain and decreases with increasing strain amplitude thereafter.

The martensitic alloys and INCRAMUTE all exhibit twin boundaries or twin-like microstructural features. It is therefore believed that these structures are responsible for the strain independent portion of the data. The responsiveness of these features may also account for the sharp threshold of the high damping response. That is to say, the boundary migration associated with high damping cannot become engaged until the twin (substructural) mechanism has become saturated. The more immediate response activation of Fe-Cr-Mo would therefore be possible due to the absence of such substructural features.

The high damping range of the martensitic alloys is believed to be caused by the intervariant boundary migration previously discussed, while that of the INCRAMUTE and Fe-Cr-Mo is related to the antiferromagnetic and ferromagnetic boundary migration, respectively.

The sharp strain-dependent peak in the Fe-Cr-Mo is believed to be due to the rapid saturation of the domain boundary migration. That is, the domain boundaries have moved to the maximum extent possible; so that additional strain can not further increase damping. In fact, they effectively become immobilized, so that damping decreases. Cyclic strain beyond the peak reverts to dominance on mechanisms associated with normal metals and SDC declines.

VI. CONCLUSIONS AND RECOMMENDATIONS

A. CONCLUSIONS

1. Cu-Al-Ni-Mn-Ti

a. For the Cu-Al-Ni based alloy, all quenching treatments produced an equivalent γ' martensitic microstructure at the scale of observation employed, but the damping properties displayed differences.

b. Low temperature aging treatments at 150°C and 200°C tended to increase the austenite start temperature (A_s).

c. Aging treatment at 200°C produced DSC endothermic peaks for the austenitizing transformation that were sharper and of greater magnitude than for either the unaged or 150°C-aged conditions.

2. INCRAMUTE

a. For this Cu-Mn alloy, the microstructures of appropriately aged samples contain minute flickering V-shaped features which exist in the Mn-rich regions, and apparently constitute the microscopic mechanism of damping.

b. The structure in the flickering V-shaped regions is FCT, but these regions are embedded in an FCC matrix without a distinct boundary between FCC and FCT. That is, there is a structural transition from FCT to FCC.

B. RECOMMENDATIONS

1. Cu-Al-Ni-Mn-Ti

a. Analysis should be conducted for a wider variety of heat treatment conditions.

b. An attempt should be made to correlate any differences in damping with changes in the DSC endothermic peaks during austenite transformation.

2. INCRAMUTE

a. Vibration analysis should be conducted with a device capable of achieving higher cyclic strain amplitude (e.g., torsion pendulum) in order to attempt to attain saturation of the antiferromagnetic domain boundary movement.

APPENDIX A

CHEMICAL COMPOSITION OF Cu-Al-Ni-Mn-Ti

LABORATORY CERTIFICATE

Anamet Laboratories, Inc.

3400 INVESTMENT BOULEVARD • HAYWARD, CALIFORNIA 94545-3811 • (415) 887-8811

Laboratory Number: 689.154
Purchase Order: N62271-89-M-2500
Requisition: N62271-89RQXB033
Date Submitted: June 14, 1989
Date Reported: June 28, 1989

Naval Postgraduate School
Receiving Officer, Bldg. 349
Monterey, CA 93943-5000
N62271-89-M-2500

SUBJECT

One metal sample was submitted for chemical analysis. The sample was identified as copper based alloy, 0.06" thick.

CHEMICAL ANALYSIS
(Reported as Wt. %)

Aluminum	(Al)	11.87
Copper	(Cu)	80.1
Manganese	(Mn)	1.83
Nickel	(Ni)	4.95
Titanium	(Ti)	1.05

This testing was performed in accordance with the purchase order.

Submitted by:

E. A. Foreman
Manager, Quality Control

bh/036

Figure A.1 Anamet Laboratories Assay of Cu-Al-Ni-Mn-Ti

APPENDIX B

Cu-Al-3Ni PHASE DIAGRAM

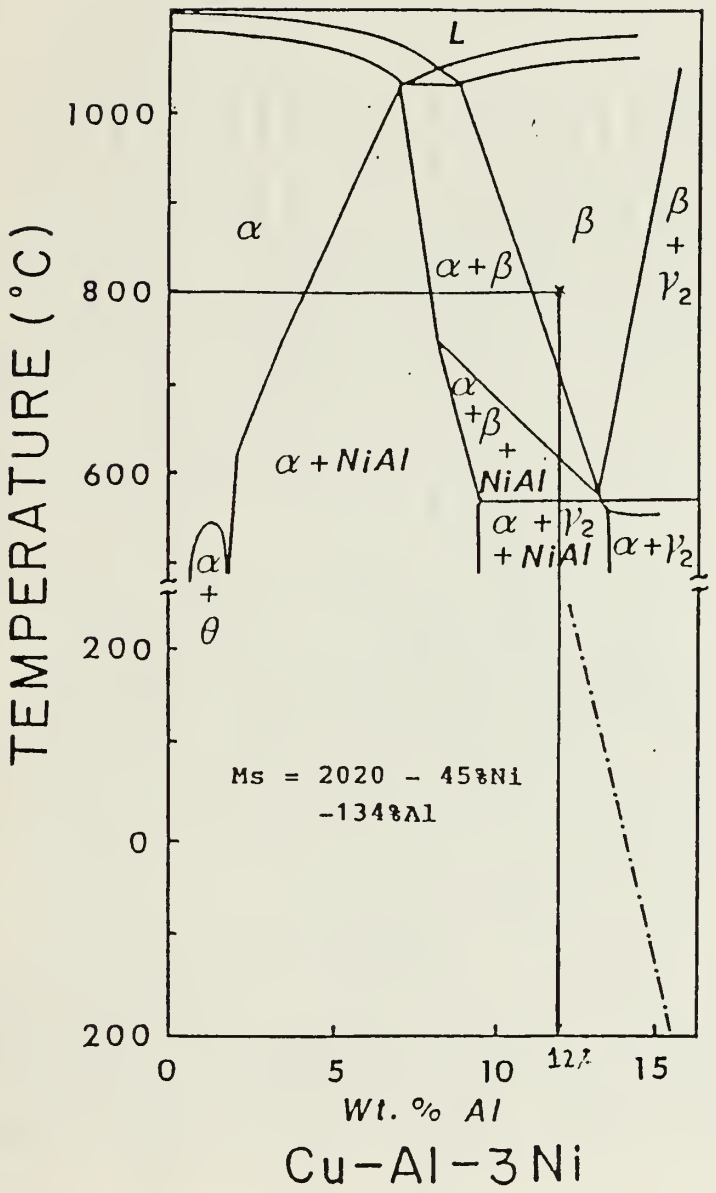

Figure B.1 Cu-Al-3Ni Phase Diagram

APPENDIX C

SPECIFIC DAMPING CAPACITY VS. CYCLIC STRAIN AMPLITUDE FOR VARIOUS ALLOYS

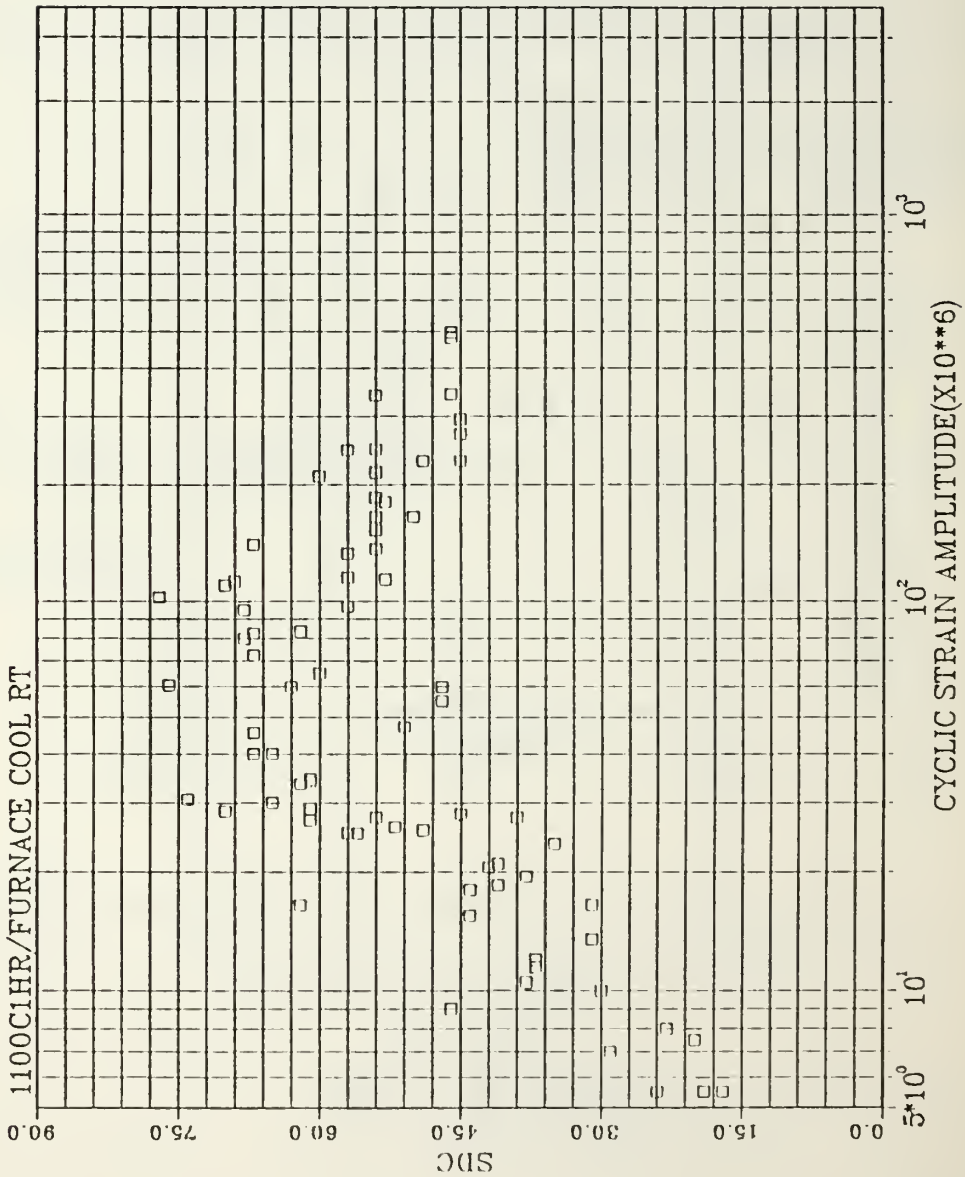

Figure C.1 SDC vs. Strain--FeCrMo

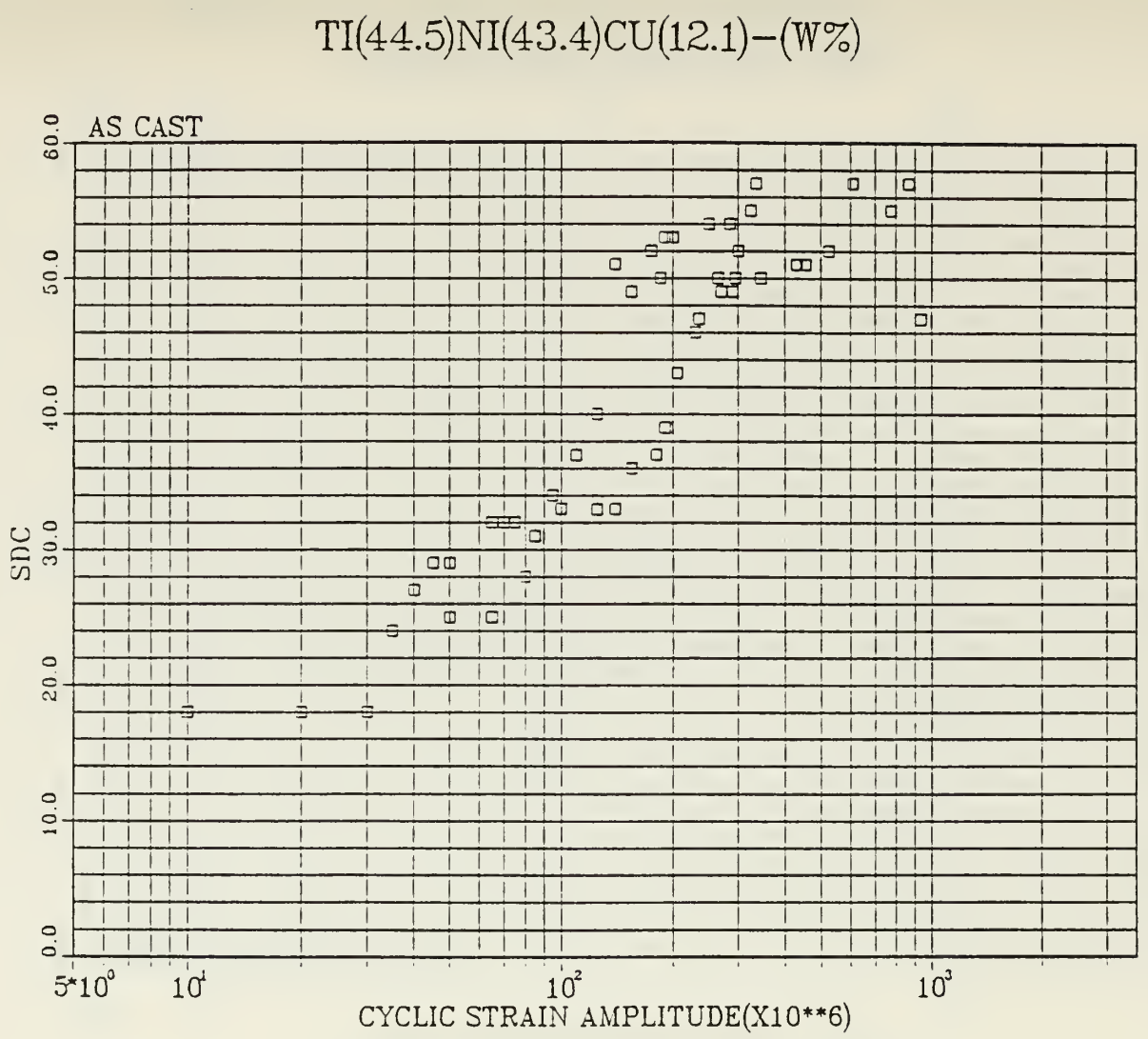

Figure C.2 SDC vs. Strain--TiNi

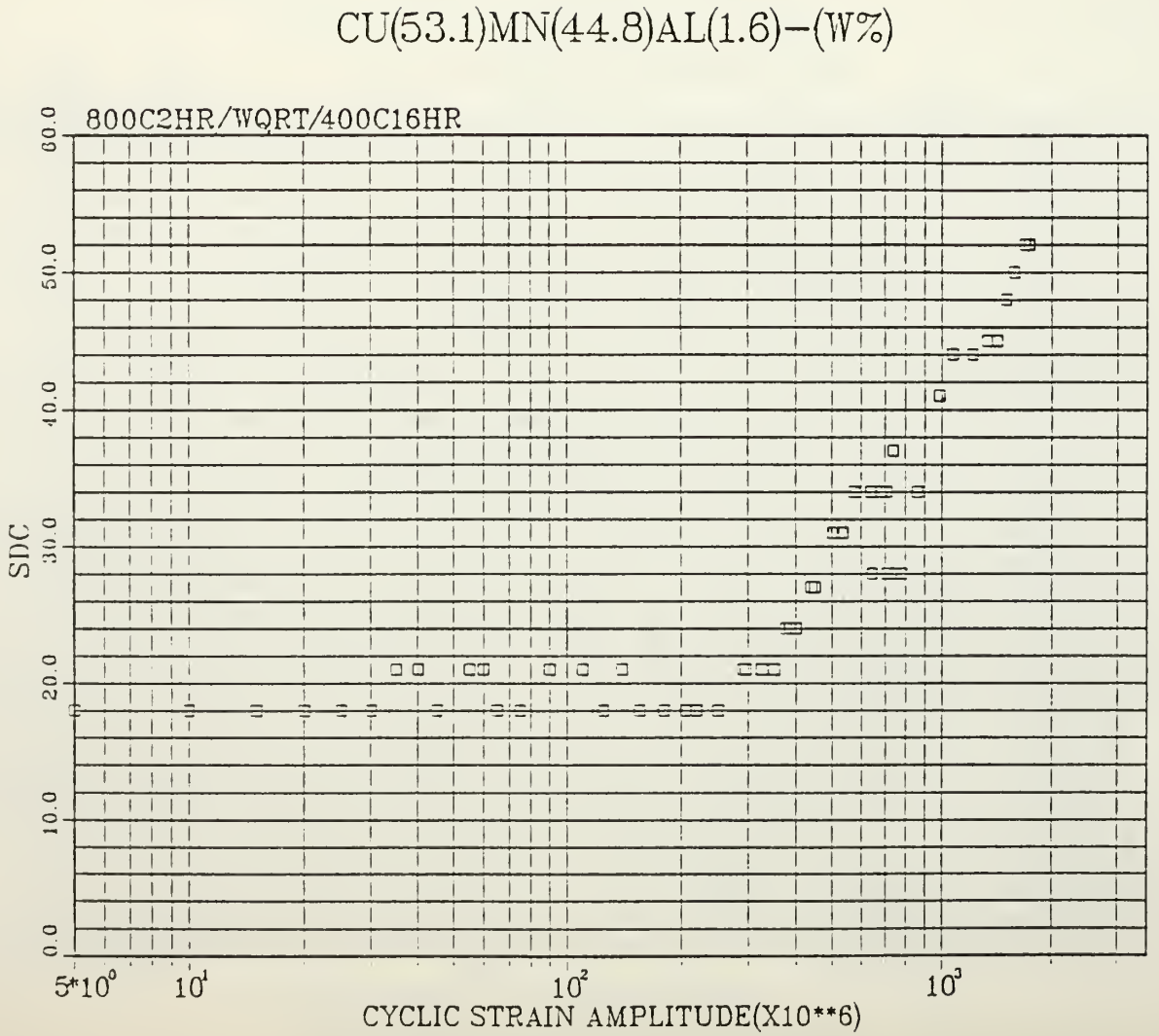

Figure C.3 SDC vs. Strain--INCRAMUTE

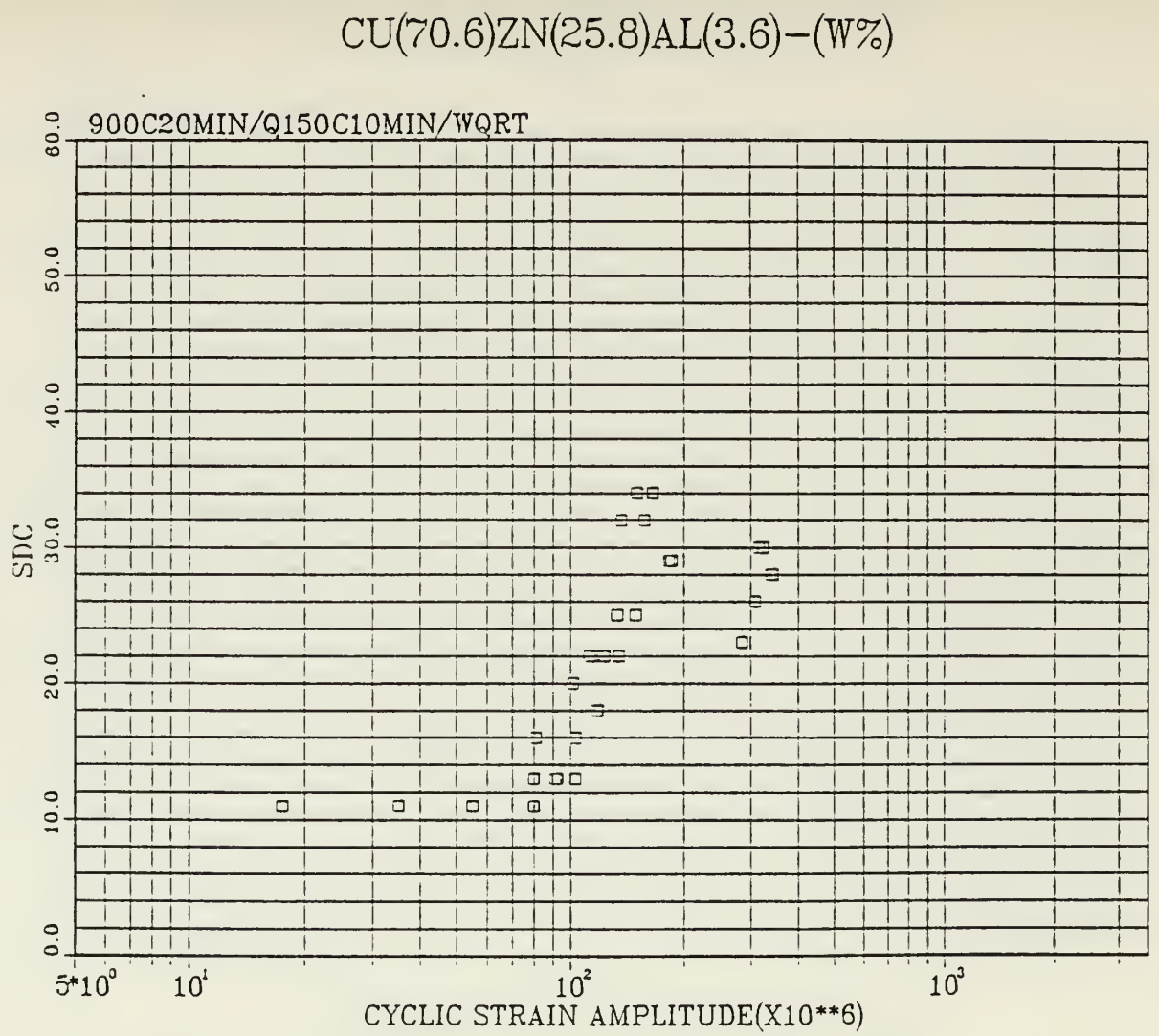

Figure C.4 SDC vs. Strain--CuZnAl

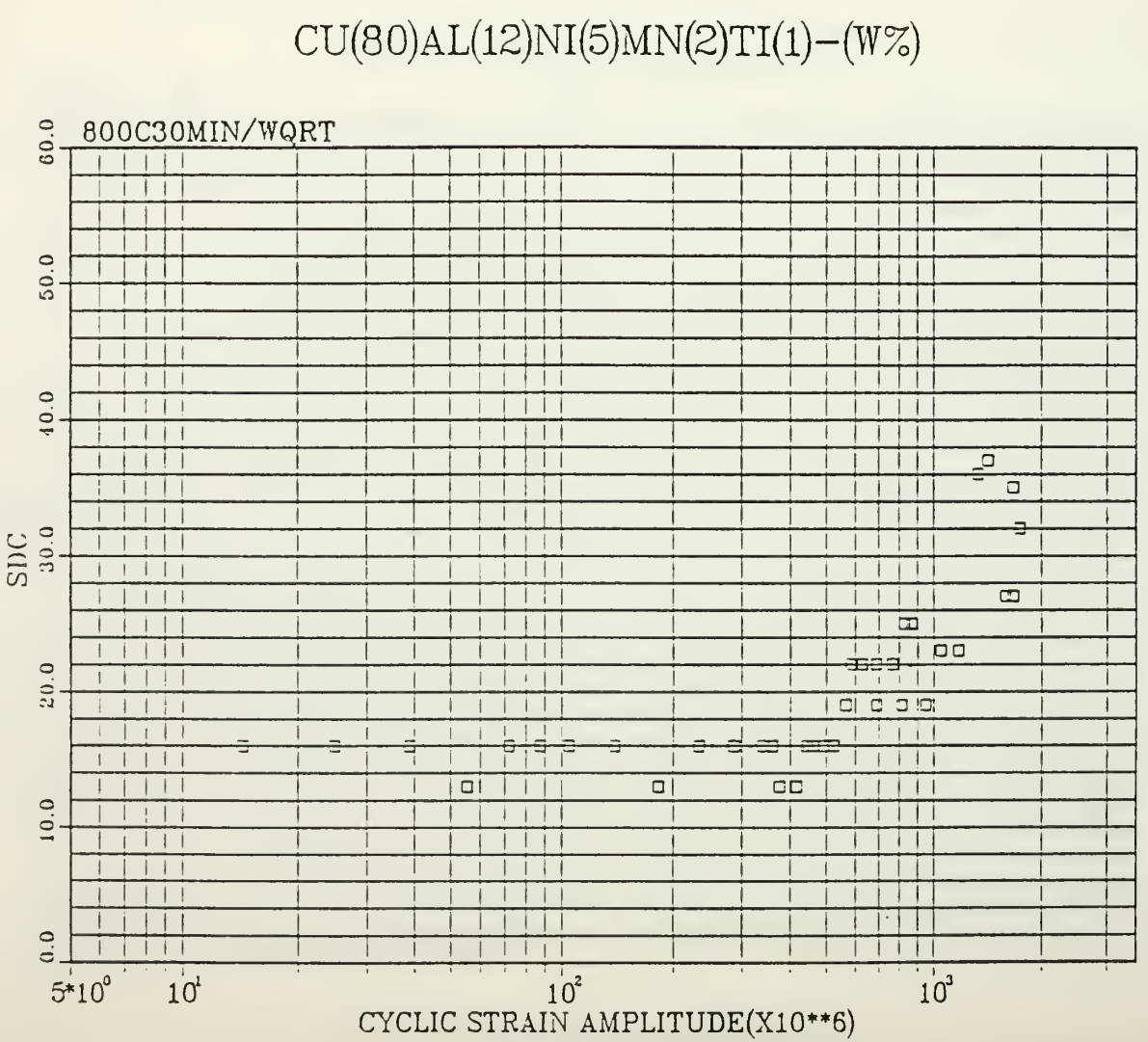

Figure C.5 SDC vs. Strain--Cu-Al-Ni-Mn-Ti
800C30MIN/WQRT

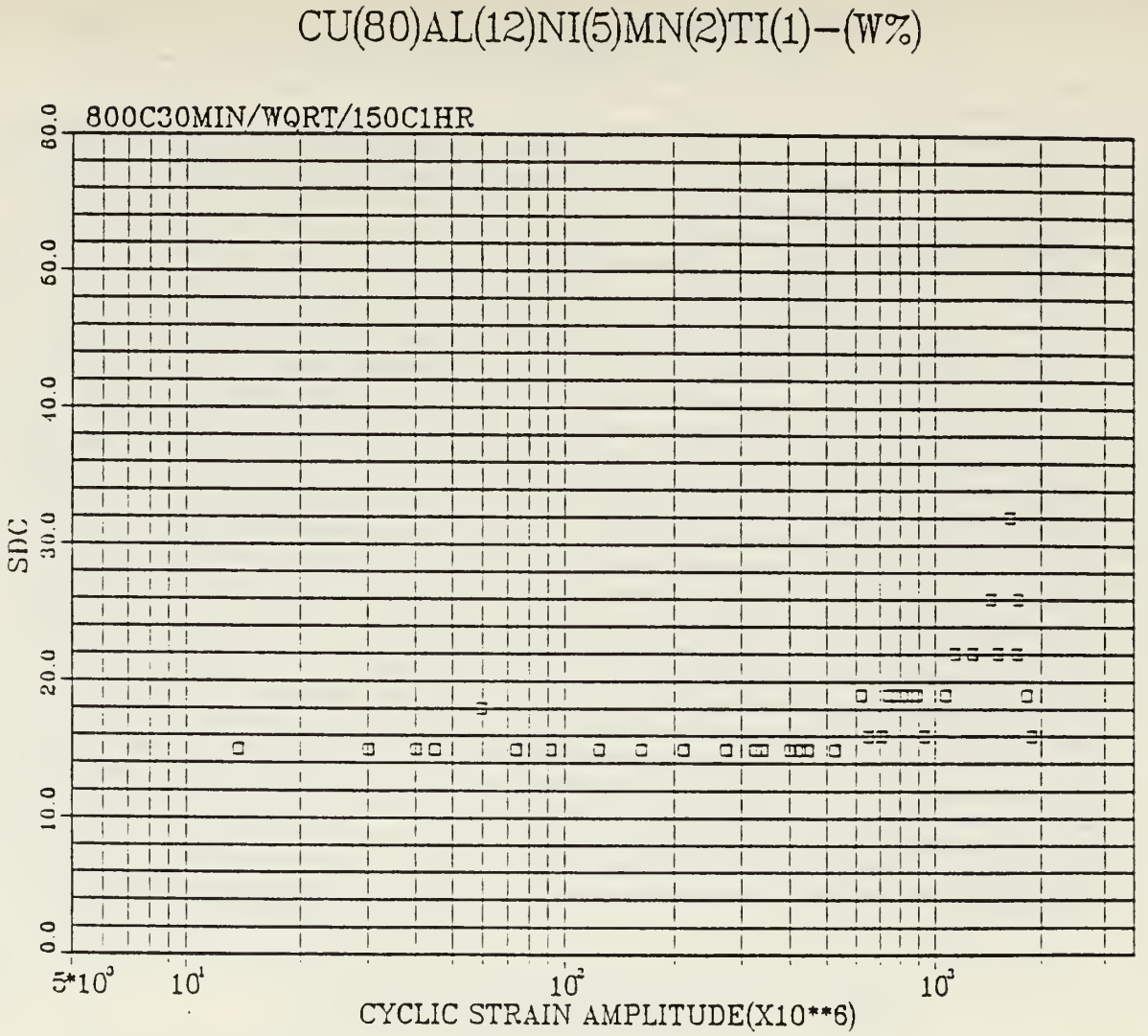

Figure C.6 SDC vs. Strain--Cu-Al-Ni-Mn-Ti
800C30MIN/WQRT/150C1HR/WQRT

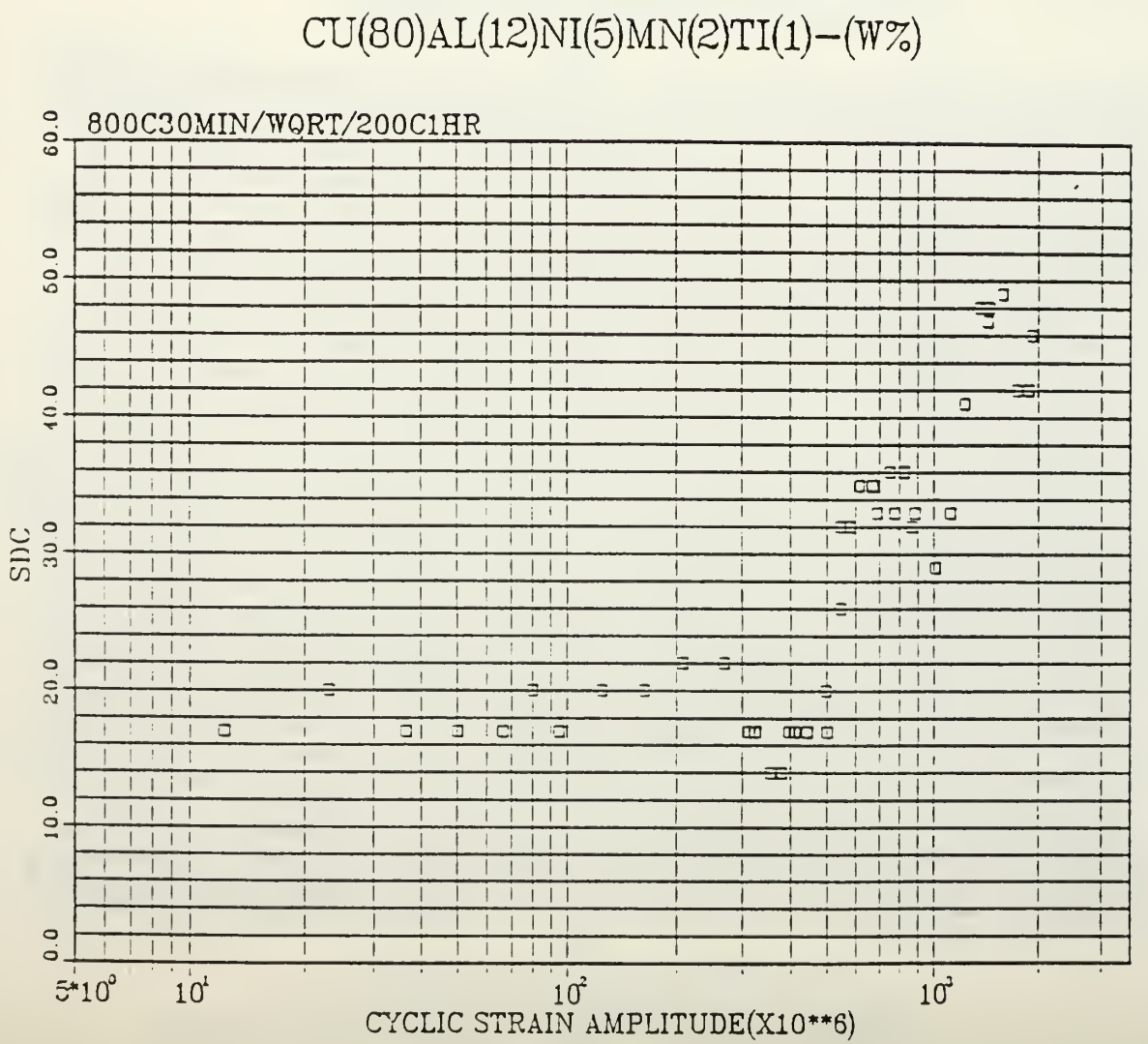

Figure C.7 SDC vs. Strain--Cu-Al-Ni-Mn-Ti
800C30MIN/WQRT/200C1HR/WQRT

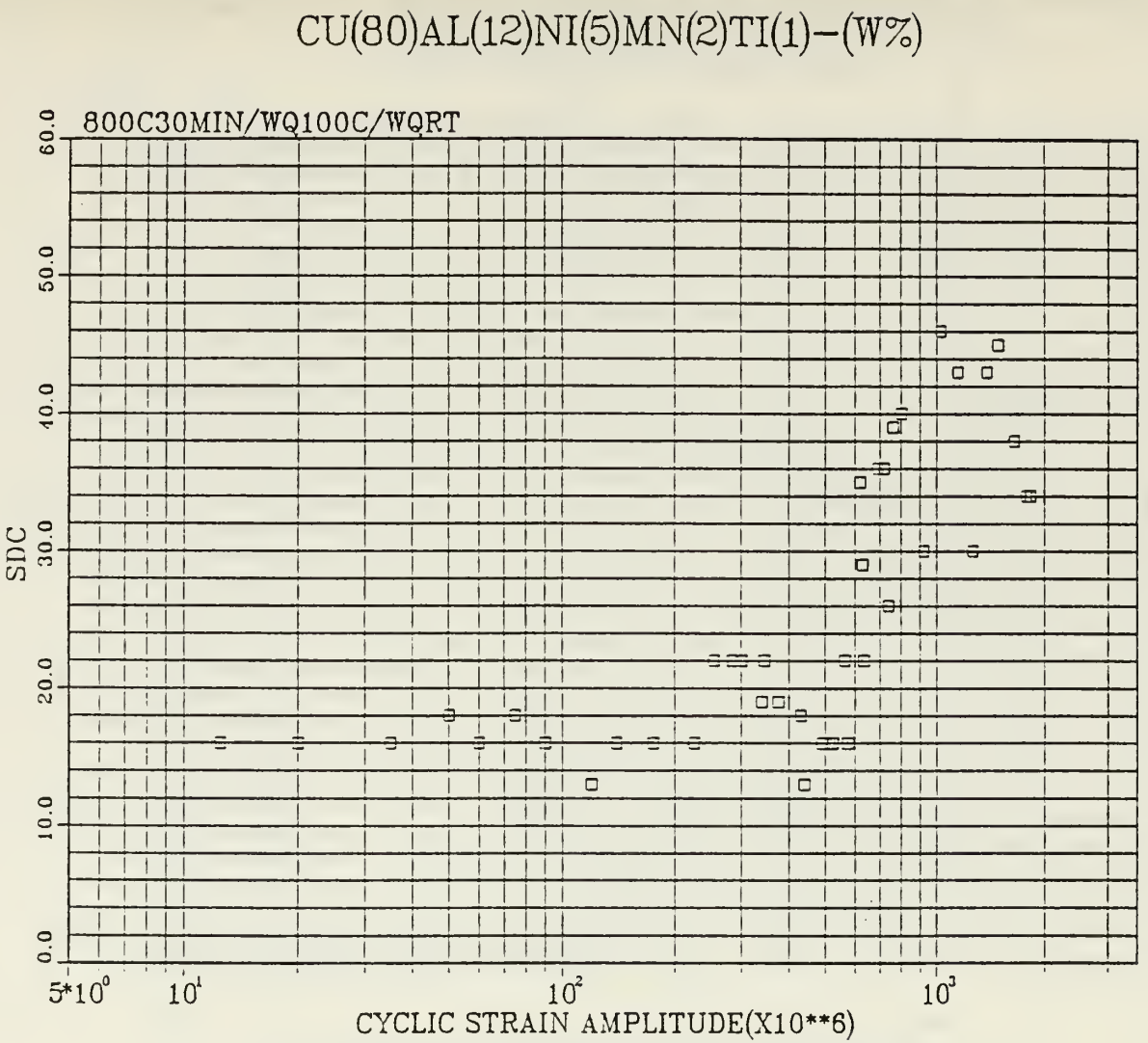

Figure C.8 SDC vs. Strain--Cu-Al-Ni-Mn-Ti
800C30MIN/WQ100C/WQRT

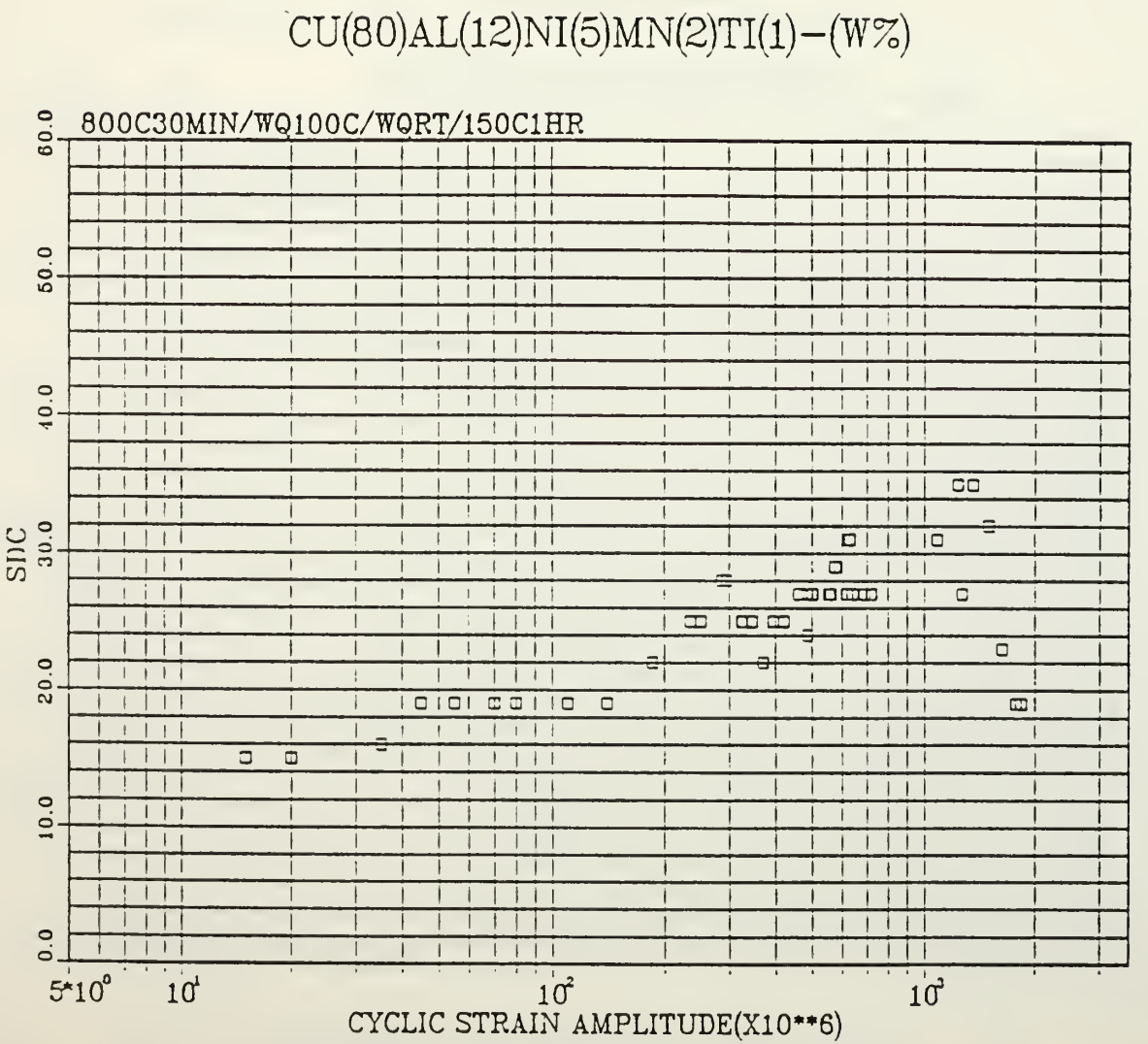

Figure C.9 SDC vs. Strain--Cu-Al-Ni-Mn-Ti
800C30MIN/WQ100C/WQRT/150C1HR/WQ100C/WQRT

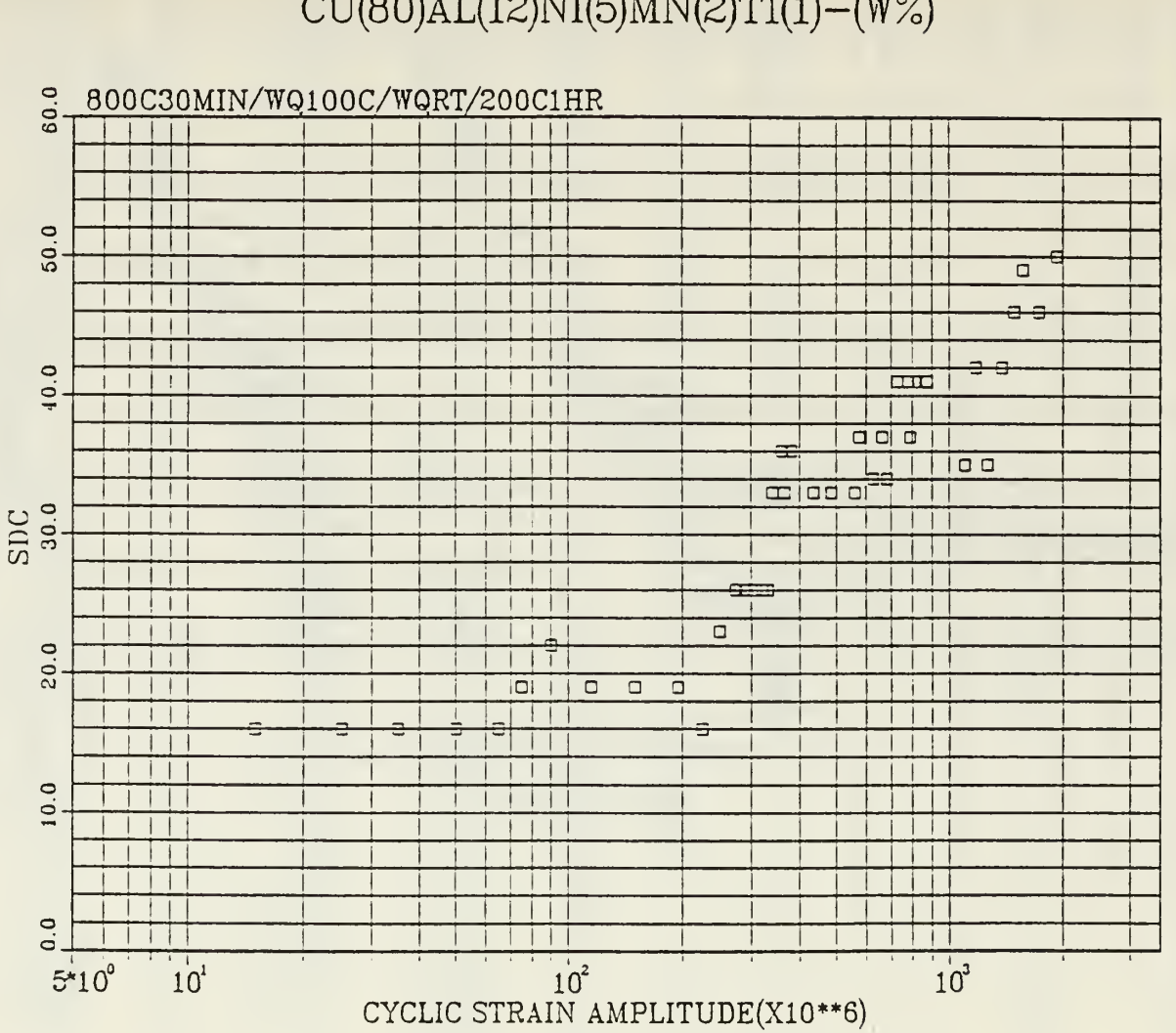

Figure C.10 SDC vs. Strain--Cu-Al-Ni-Mn-Ti
800C30MIN/WQ100C/WQRT/200C1HR/WQ100C/WQRT

APPENDIX D

COMPARISON OF DSC AUSTENITIC PEAKS FOR 150°C AND 200°C AGED Cu-Al-Ni-Mn-Ti

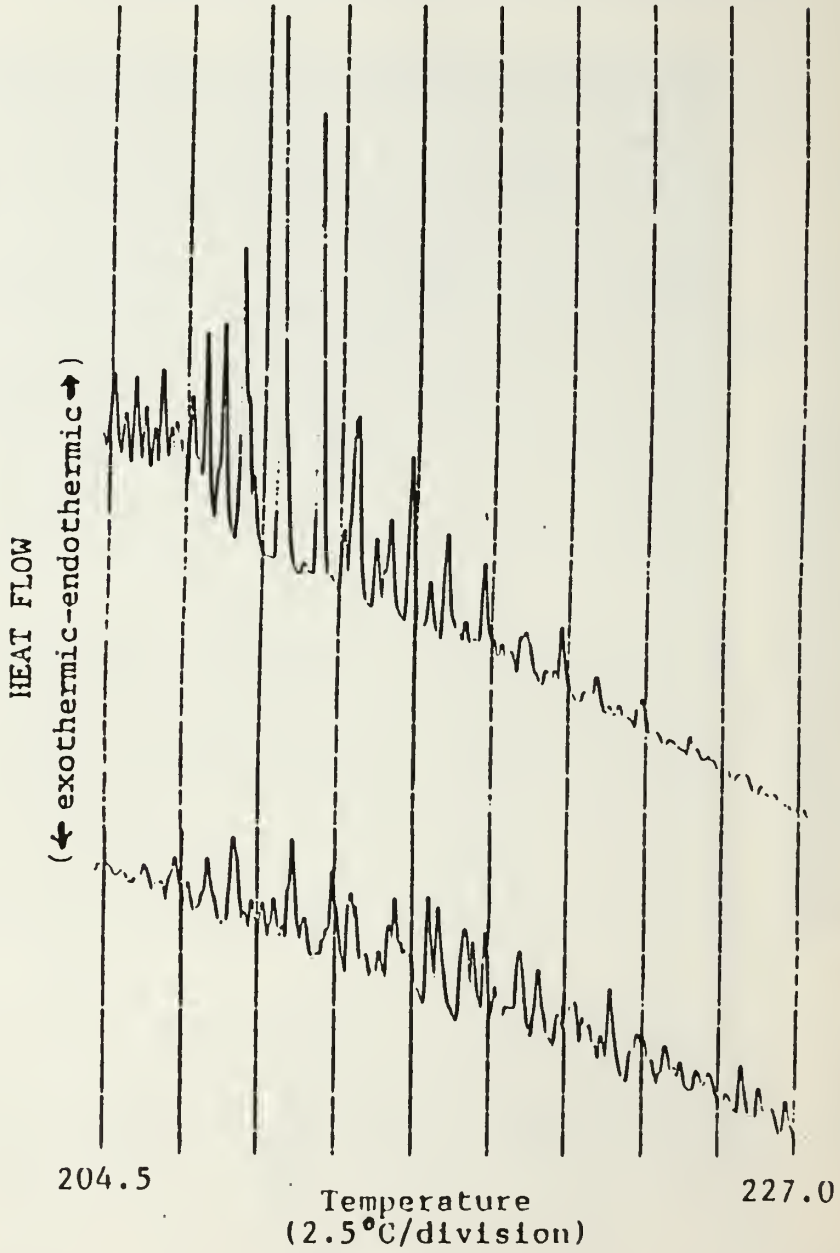

Figure D.1 Austenitic Endothermic Peaks in Aged Cu-Al-Ni-Mn-Ti. Upper Curve 200° Age. Lower Curve 150° Age.

LIST OF REFERENCES

1. Eisenstadt, M.M., Introduction to the Mechanical Properties of Materials, p. 171, MacMillan, 1971.

2. Friedel, J., Dislocations, Addison-Wesley, 1964.

3. Otsuka, K. and Shimizu, K., "Pseudoelasticity," Metals Forum, Vol. 4, No. 3, pp. 142-152, 1981.

4. Verhoeven, I.D., Fundamentals of Physical Metallurgy, pp. 457-500, John Wiley and Sons, 1975.

5. Wayman, C.M., "The Shape Memory Effect," Metals Forum, Vol. 4, No. 3, pp. 135-141, 1981.

6. Feynman, R.P., Leighton, R.B., and Sands, M., Lectures on Physics, Addison-Wesley, 1964.

7. Kittel, C., Introduction to Solid State Physics, 3rd Ed., John Wiley and Sons, 1966.

8. Meyers, M.A., and Chawla, K.K., Mechanical Metallurgy Principles and Applications, Prentice-Hall, 1984.

9. Roey, K., and Perkins, J., A Comparison of CuAlNi and Other High Damping Alloys for the Purpose of Ship Silencing Applications, Master's Thesis, Naval Postgraduate School, Monterey, California, September 1989.

10. Roskusich, J., and Perkins, J., Damping Behavior of INCRAMUTE: Strain Dependence and Heat Treatment Effects, Master's Thesis, Naval Postgraduate School, Monterey, California, September 1986.

11. Shetky, L.M., and Perkins, J., "The 'Quiet' Alloys," Machine Design, pp. 202-206, 6 April 1978.

12. Mayes, L., and Perkins, J., An Electron Microscope Study of Tweed Microstructures and Premartensitic Effects in High Damping 53Cu45Mn2Al Alloy, Master's Thesis, Naval Postgraduate School, Monterey, California, March 1988.

INITIAL DISTRIBUTION LIST

		No. Copies
1.	Defense Technical Information Center Cameron Station Alexandria, Virginia 22304-6145	2
2.	Library, Code 0142 Naval Postgraduate School Monterey, California 93943-5002	2
3.	Professor Jeff Perkins, Code 69Ps Department of Mechanical Engineering Naval Postgraduate School Monterey, California 93943-5000	3
4.	LCDR Kenneth P. Roey 949 Nugent Drive Chesapeake, Virginia 23320	1
5.	Mrs. Catherine Wong, Code 2812 David Taylor Naval Ship R&D Center Annapolis, Maryland 21402	3
6.	Department Chairman, Code 69Hy Department of Mechanical Engineering Naval Postgraduate School Monterey, California 93943-5000	1
7.	Naval Engineering Curricular Officer, Code 34 Naval Postgraduate School Monterey, California 93943-5000	1
8.	Dr. Ming Wu Memory Metals, Inc. 83 Keeler Ave. Norwalk, Connecticut 06854	1
9.	Naval Sea Systems Command Code 92R Washington, D.C. 20362-5101	1
10.	Dr. Kam Ng Code 8322 Bldg. 1246 Naval Underwater Systems Center Newport, Rhode Island 02841	1

11. LCDR Peter F. Rappeline 3
522 Kalolina Street
Kailua, Hawaii 96734

Thesis
R2198
c.1

Rappeline
The microstructural basis of damping in high damping alloys.

Thesis
R2198
c.1

Rappeline
The microstructural basis of damping in high damping alloys.

AMERICAN BINDERY
TOPEKA KANSAS

thesR2198
The microstructural basis of damping in
3 2768 000 86515 8
DUDLEY KNOX LIBRARY